ISIJ International, Vol. 49 (2009), No. 10, pp. 1568–1574

Numerical Analysis on Columnar-to-equiaxed Transition of δ-Ferrite Dendrite in Carbon Steel Induced by Titanium Carbonitride Particles

Munekazu OHNO and Kiyotaka MATSUURA

Division of Materials Science and Engineering, Graduate School of Engineering, Hokkaido University, North 13 West 8, Sapporo 060-8628 Japan.

(*Received on April 10, 2009; accepted on June 23, 2009*)

Dendrite growth simulations have been performed to analyze Columnar-to-Equiaxed Transition (CET) of δ-ferrite dendrite structure triggered by fine particles of a primary Ti(C, N) crystal. The CET position estimated by Hunt's criterion and the present simulation indicated that the existence of a large number of the Ti(C, N) particles gives rise to the CET of the dendrite structure even in the vicinity of the mold wall under the present casting condition. Furthermore, the capability of the Ti(C, N) leading to the CET was discussed in the light of the different number of Ti(C, N) particles and the different thickness of cast ingot. It was shown that a sufficient number of Ti(C, N) leads to the formation of fully equiaxed dendrite structure irrespective of the ingot thickness.

KEY WORDS: columnar-to-equiaxed transition; hyperperitectic steel; titanium carbonitride; casting; solidification; simulation; dendrite structure.

1. Introduction

Steep temperature gradient in solidifying steel leads to columnar austenite (γ) crystal grain structure developed from the surface toward the center of the continuously cast slabs or billets. Formation of fine equiaxed γ grain structure is of critical importance in steel industries to prevent surface cracking and harmful effects on mechanical properties at high temperatures originating from the coarse columnar structure.[1,2] In our recent study on the casting process of a hyperperitectic steel,[3] it has been demonstrated that the addition of a certain amount of titanium results in fully equiaxed fine γ grain structure over the whole cast ingot. The microstructural observations indicated that the formation of the equiaxed γ-grain structure should be essentially related to the Columnar-to-Equiaxed Transition (CET) of ferrite (δ)-dendrite structure. The fully equiaxed δ-dendrite structures were observed in a range of the titanium addition where titanium carbonitride, Ti(C, N), is expected to exist as the primary crystal before the δ-dendrite solidification based on the thermodynamic consideration. It has been reported that the Ti(C, N) is quite effective in promoting the heterogeneous nucleation of δ-ferrite because of a low disregistry with the δ-ferrite phase.[4,5] Furthermore, the metallographic analyses in early works[6,7] suggest that the Ti(C, N) crystal leads to the CET of δ solidification.

The occurrence of CET phenomenon depends largely on several factors such as the temperature field, undercooling for the dendrite growth and nucleation event of the equiaxed dendrite. Ahead of the columnar dendrite, there exists a constitutional undercooling region. When the nucleation of the equiaxed dendrite occurs in such an undercooling region, the further development of the columnar dendrite is blocked by the equiaxed dendrites, leading to the CET. Based on this picture, Hunt developed an analytical model to provide a criterion for the occurrence of CET.[8] While several improvements have been presented[9–11] and more detailed simulations have been performed to directly describe the CET,[12–15] it is considered that the Hunt's model should be successful to capture the essence of the CET phenomenon. According to the Hunt's model, the fully equiaxed growth occurs when the temperature gradient at the solidification front, G, satisfies the following condition,

$$G < 0.617 N_0^{1/3} \left\{ 1 - \left(\frac{\Delta T_N}{\Delta T_t} \right)^3 \right\} \Delta T_t \quad \text{.....(1)}$$

where N_0 is the number of the nucleation sites for the equiaxed dendrites, ΔT_N is the undercooling for the nucleation of equiaxed dendrite and ΔT_t is the undercooling for the columnar dendrite growth. From the above equation, one can readily grasp that the large value of N_0 and/or small value of ΔT_N leads to the CET even under steep temperature gradient.

As mentioned above, several works based on the microstructural observations have indicated that the Ti(C, N) crystal triggers the CET of δ solidification.[3,6,7] It has been reported that the nucleation undercooling of δ-Fe on Ti(C, N) is just 1.8°C,[4] which indicates a high ability of the

Ti(C, N) giving rise to the CET of δ dendrite solidification. When the values of N_0 and ΔT_N are given, one can predict the occurrence of the CET based on the relation between G and ΔT_t (or the growth velocity of columnar dendrite described as a function of ΔT_t, $V(\Delta T_t)$) within the Hunt's model. It should be pointed out that G and ΔT_t (and V) are essentially time-dependent quantities during the casting process and the analysis of the CET requires such a time dependency to be addressed in detail.

The main objective of this study is twofold; one is to substantiate the occurrence of the CET of δ dendrite morphology induced by the primary Ti(C, N) in the light of the time-dependent behavior of G–V relation during the casting process and the other is to analyze the capability of Ti(C, N) giving rise to the CET under various casting conditions. To this end, we carry out a columnar dendrite growth simulation describing the time-dependent behavior of G–V relation. The input parameters for the simulation are obtained from the results of casting experiment. The relation between our calculated results and the Hunt's criterion suggests that the Ti(C, N) particles induce the CET of δ dendrite morphology in the vicinity of the side surface of the ingot, which is fairly consistent with the metallographic observations. Finally, the capability of the Ti(C, N) giving rise to the CET is discussed in terms of several solidification conditions with the different number of Ti(C, N) particles and the different cooling conditions. In the conventional continuous casting process of the steel, the slab thickness is one of parameters to change the cooling rate of the cast. Therefore, we will discuss the occurrence of the CET in the different cast thickness. One will see that a sufficient number of the Ti(C, N) particles lead to the formation of the equiaxed dendrite over almost the entire cast ingot irrespective of the cast thickness.

2. Experimental

The casting experiments were carried out for samples of S45C steel with and without titanium addition. The S45C steel employed in this study consists of 0.436 wt% C, 0.204 wt% Si, 0.679 wt% Mn, 0.014 wt% P, 0.014 wt% S, 0.025 wt% Al, 0.0015 wt% O and 0.0052 wt% N. The amount of titanium addition was set to be 0.15 wt% at which Ti(C, N) is the primary crystal according to the calculated phase diagram.[3] As discussed in our previous report,[3] the equiaxed dendrite structure will develop over the entire sample with addition of 0.15 wt% Ti. Phosphorus was added in the samples by 0.02 wt% to observe the δ-dendrite solidification structure. The sample of about 250 g was melted at 1 550°C in an SiC electric furnace filled with argon gas with 99.999% purity. The melt was held for 1 h at 1 550°C and it was then cast into a steel mold. The detail of the steel mold used in this study can be found in the previous report.[3]

The cast ingots were a rectangular prism with 40 mm in width, 20 mm in thickness and 40 mm in height. The observation was made on a horizontally sectioned plane at the height of 20 mm. The dendrite structure was investigated by an optical microscope after polishing and etching in an Oberhöffer's reagent. A Scanning Electron Microscope (SEM) and an Electron Probe Micro-Analyzer (EPMA) were also utilized to examine the Ti(C, N) particles. As demonstrated later in the fourth section, the columnar dendrite develops from the side surface of the ingot toward the center along the thickness direction without titanium addition, except for the edge parts in the width direction of the ingot. Therefore, it may be allowed to take into account only the one-dimensional heat flow along the thickness direction from the inward of ingot to the mold wall in the discussion. We take this fact as a basis for simplifications in the numerical simulation as detailed in the following section.

In addition to the metallographic investigations, the temperature measurement was carried out during the casting process of the S45C steel without titanium addition. To monitor the temperature of the cast sample during cooling, the type-B thermocouple was inserted into the center of the mold cavity from the open upper side of the mold. The tip of the thermocouple was located at the center of the cast and it was thinly coated with Al_2O_3 cement to prevent a reaction with the molten steel. The comparison between the microstructures of samples with and without the thermocouple showed that the thermocouple inserted in the cast does not affect the solidification microstructure in the observation area. The cooling curve was utilized to determine the heat transfer coefficient for the simulation of the dendrite growth.

3. Calculation Details

As mentioned in the introduction, the temperature gradient at the solidification front, G, and the dendrite tip velocity, V, are the central quantities in the Hunt's criterion. Although the CET phenomena have been directly described by means of several simulation approaches such as the Phase-field method[12] and the Cellular Automaton (CA) model,[13,14] a simplified simulation is performed in this study, focusing on only the time-dependences of G and V during the columnar dendrite growth. Instead of directly describing the CET process, then, we analyze the occurrence of the CET by comparing the G–V relation with the Hunt's criterion. This scheme based on the analytical CET model and the calculated G–V relation is essentially equivalent to the one discussed by Kurz *et al.*[16]

The simulation method for G–V relation employed in this work basically corresponds to the CA model for the mesoscopic solidification process.[17,18] Within the CA model, the dendrite tip velocity is described as a function of local temperature, for example, based on the Kurz–Giovanola–Trivedi (KGT) model.[19] Within the KGT model, the total undercooling of the dendrite growth front, ΔT_t, is written as a sum of different contributions,

$$\Delta T_t = \Delta T_c + \Delta T_r + \Delta T_k \quad \text{.....(2)}$$

where ΔT_c, ΔT_r, and ΔT_k are the undercooling contributions originating from solute diffusion, solid–liquid interface curvature and attachment kinetics, respectively. The solutal undercooling, ΔT_c, is expressed as

$$\Delta T_c = m_v C_0 \left(1 - \frac{1}{1 - (1 - k_v) Iv[P_C]} \right) \quad \text{.....(3)}$$

Table 1. Parameters employed in the present work. The thermodynamic quantities were determined from the Calphad method.[21] The other parameters were taken from Refs. 24), 25).

Parameter	Unit	Values
Concentration of carbon, C_0	wt%	0.45
Melting temperature of pure Fe, T_0	°C	1538
Peritectic reaction temperature, T_p	°C	1495
Liquids slope, m	°C /wt%	−87.45
Equilibrium partition coefficient, k_e	-	0.17
Diffusion constant of liquid, D	m^2/s	2.0×10^{-8}
Gibbs-Thomson coefficient, Γ	°C·m	2.2×10^{-7}
characteristic length scale for solute trapping, a_0	m	1.0×10^{-9}
Linear kinetic coefficient, μ	s/(°C·m)	0.76
Thermal conductivity, $K=f_L\cdot K_L+f_s\cdot K_s$	W/(m·K)	
Thermal conductivity for liquid, K_L	W/(m·K)	$21.5\times10^{-3}(T-1818)+33.3$
Thermal conductivity for solid, K_s	W/(m·K)	$1.28\times10^{-2}T+10.9$
Undercooling degree of δ-Fe on Ti(C,N), ΔT_n	°C	1.8

where C_0 is the solute concentration and $Iv[P_C]$ is the Ivantosov function with the solutal Péclet number, P_C. In Eq. (3), m_v, k_v and P_c are, respectively, given as

$$m_v = m\frac{1-k_v(1-\ln(k_v/k))}{1-k} \quad \text{.....(4)}$$

$$k_v = \frac{k+a_0\cdot V/D}{1+a_0\cdot V/D} \quad \text{.....(5)}$$

$$P_C = \frac{RV}{2D} \quad \text{.....(6)}$$

where m is the liquidus slope, k is the equilibrium partition coefficient of the solute element between the solid and liquid, a_0 is characteristic length scale for solute trapping, V is dendrite tip velocity, R is the curvature radius at the dendrite tip and D is the diffusion coefficient of the solute atom in the liquid. Within the marginal stability criterion,[20] the following relation is held

$$R = \left[\frac{\Gamma}{\sigma^*(m_v\zeta_c G_c - G)}\right]^{1/2} \quad \text{.....(7)}$$

where Γ is the Gibbs–Thomson coefficient, σ^* is a stability constant given by $1/(4\pi)^2$, G is the temperature gradient and ζ_c is expressed as

$$\zeta_c = 1-\frac{2k_v}{\{1+(2\pi/P_c)^2\}^{1/2}-1+2k_v} \quad \text{.....(8)}$$

The curvature undercooling, ΔT_r, is given by

$$\Delta T_r = \frac{2\Gamma}{R} \quad \text{.....(9)}$$

The attachment kinetic undercooling, ΔT_k, is described as follows

$$\Delta T_k = \frac{V}{\mu} \quad \text{.....(10)}$$

where μ is the linear kinetic coefficient.

From the equations thus described, the dendrite tip velocity, V, is calculated as a function of the total undercooling for the dendrite growth, $V(\Delta T_t)$. By coupling the following heat conduction equation, then, one can describe the evolution process of the dendrite structure

$$\rho\cdot c_p\frac{\partial T}{\partial t} = \nabla(k\nabla T)+\rho\cdot\Delta H\frac{\partial f_s}{\partial t} \quad \text{.....(11)}$$

where ρ is the density, c_p is the specific heat capacity, K is the thermal conductivity, f_s is the solid fraction and t is the time. It should be mentioned that the dendrite tip velocity $V(\Delta T_t)$ is essentially dependent on the temperature gradient G. As is common practice in the CA study, however, the effect of G on $V(\Delta T_t)$ is not taken into account in the present simulation, since the variation of $V(\Delta T_t)$ with respect to G is negligibly small in the range of G of our focus. The parameters employed in this work are listed in **Table 1**. In this study, the thermodynamic quantities of each phase such as the heat capacity, the latent heat and also the solid fractions of δ and γ phases were calculated as functions of temperature based on the Calphad approach with the thermodynamic database reported in Ref. 21).

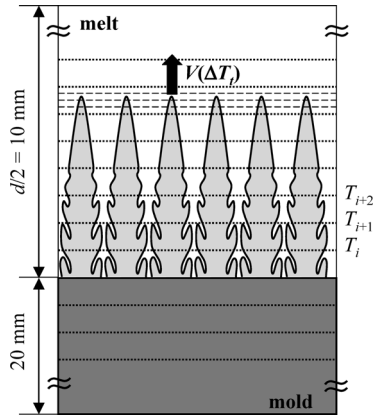

Fig. 1. Schematic drawing of simulation system.

The simulation system is schematically illustrated in **Fig. 1**. A detailed and realistic description of the solidification microstructure requires the three dimensional simulation to be performed with a high accuracy. However, it is computationally quite demanding. Our main concern is not the detailed morphology and size of the microstructure but the time-dependent behavior of the G–V relation. As already

mentioned, it is allowed to consider only the one-dimensional heat flow under the present casting condition. Accordingly, our focus is directed to one-dimensional simulation. The grid distance of $\Delta x = 5 \times 10^{-5}$ m is employed for the calculation of the temperature field. Since our concern here is limited to the growth process of the columnar dendrite from the mold wall, we initially assign the nucleus at the grid point on the mold wall, which starts to grow based on the KGT model when the temperature at the corresponding grid point becomes lower than the liquidus temperature. The temperature at the dendrite tip position is calculated by the linear interpolation using the temperatures at the nearest neighbor grid points. The volume fraction of solid is calculated based on the Scheil equation[22] at the grid points where the dendrite tip passed through. It is to be noted that the formation and growth of the γ-phase are not explicitly dealt with in this method and, instead, the development of γ phase is described as the evolution of solid fraction below the peritectic temperature.

It should be pointed out that the Hunt's model is based on several assumptions such as quasi steady-state growth condition and mechanical block mechanism. It cannot be strongly assured that these assumptions are validated in the present casting condition. However, several studies on the CET[12,16] suggest that the Hunt's model is basically able to describe the CET phenomena pertinently in spite of the above-mentioned assumptions. Therefore, by allowing uncertainty in numerical value associated with these assumptions, we attempt to analyze the CET based on the Hunt's model in this study.

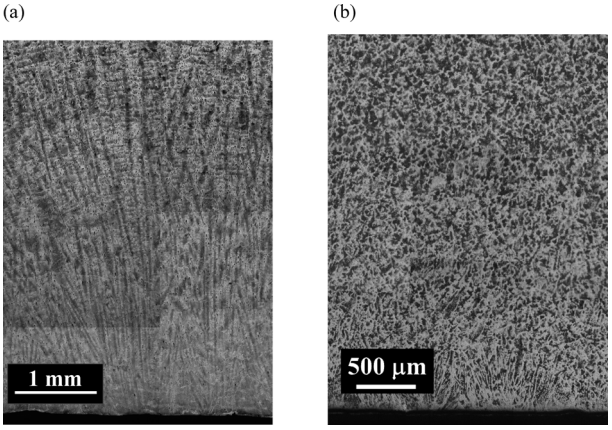

Fig. 2. Dendrite structures of samples (a) without Ti and (b) with 0.15 wt% Ti observed on the horizontal section of the rectangular ingot. The bottom of the micrographs corresponds to the side surface of the ingot.

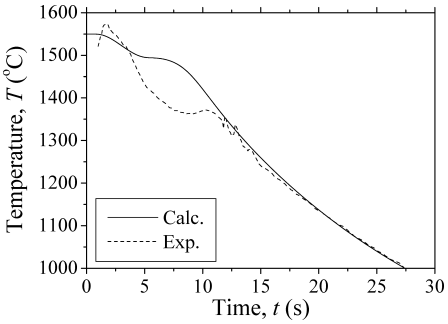

Fig. 3. Cooling curves at the center of the ingot during the casting process. The solid and dashed lines represent the simulated and the experimental results, respectively.

4. Results and Discussion

The δ-dendrite structures in the samples without and with titanium addition are demonstrated in **Figs. 2**(a) and 2(b), respectively. The vertical direction of the micrographs is the thickness direction. The bottom of the micrographs corresponds to the side surface of the ingot. It can be seen in this figure that titanium addition leads to a striking difference in the δ dendrite structure, as was discussed in Ref. 3). In the sample without the titanium addition, the columnar dendrites develop from the side surface to the inward of ingot along the thickness direction, which is a consequence of one dimensional heat flow from the inward to the side surface of the ingot. In the sample with 0.15 wt% Ti, on the other hand, the equiaxed δ-dendrites form even in the vicinity of the side surface. Although the CET position cannot be clearly defined in Fig. 2(b), the CET seems to occur at a distance of less than 0.5 mm inward from the side surface. The calculated phase diagram showed that the Ti(C, N) phase crystallizes from the melt prior to the δ solidification in the sample with 015 wt% Ti.[3] In fact, faceted particles of Ti(C, N) with an edge length of about 2 μm were uniformly dispersed in the sample with the titanium addition. Such a primary Ti(C, N) phase is considered to induce the CET of δ solidification.

Figure 3 shows the calculated and experimental cooling curves at the center of the ingot during the casting process without the titanium addition. Although the following discrepancies exist, the calculated cooling curve (solid line) is not significantly different from the experimental curve (dashed line). In the experimental curve, the temperature in a very early period becomes slightly higher than the initial holding temperature, 1 550°C, since the temperature distribution in the furnace is not completely uniform. The recalescence is observed around 1 370°C in the experimental curve, which may represent the formation of γ phase with large undercooling. This is not described in the calculated result, since the undercooling of the nucleation of γ phase is not taken into account and the γ phase starts to develop at the peritectic temperature, $T_p = 1\,495$°C in the simulation. It should be noted that our focus is the δ solidification process and the undercooling phenomenon of γ formation is almost irrelevant to our discussion for the CET which occurs in a very early period of the casting process. In the experimental curve, the recalescence due to δ solidification is not clearly observed. However, from the derivative of the experimental cooling curve, the temperature at which δ solidification starts was estimated to be about 1 495°C at $t \approx 4$ s. In addition, the cooling rate, $\dot{T}$, at 5 mm inward from the side surface of the ingot is calculated to be 17°C/s, which is quite comparable to the experimentally estimated value of 15°C/s based on the empirical relation,[23] $\lambda_{DAS} = 683(60\dot{T})^{-0.37}$ with the measured secondary dendrite arm spacing, $\lambda_{DAS} = 55\,\mu$m. Hence, although there are discrepancies between the experimental and calculated cooling curves in the center part of sample as shown in Fig. 3, it is considered that the calculated result reasonably describes the experimental cooling behavior during columnar δ den-

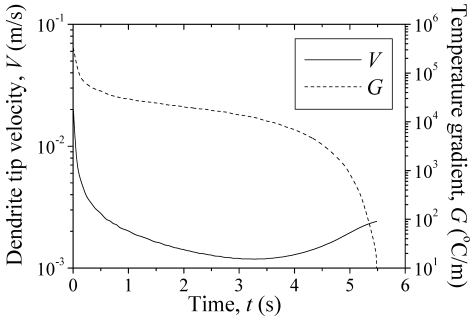

Fig. 4. Temporal evolutions of dendrite tip velocity (solid line) and the temperature gradient (dashed line) at the δ/L solidification front. The left vertical axis represents the velocity, while the right axis specifies the temperature gradient.

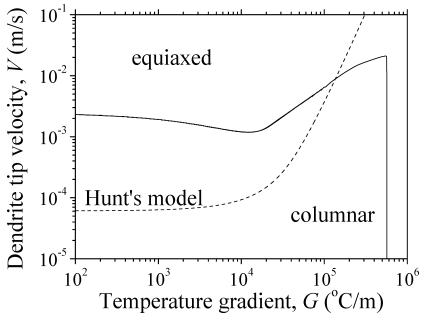

Fig. 5. Relation between dendrite tip velocity and temperature gradient at the solidification front. The dashed line indicates the result of Hunt's model calculated with $N_0=8\times10^{12}\,\mathrm{m}^{-3}$ and $\Delta T_N=1.8$°C.

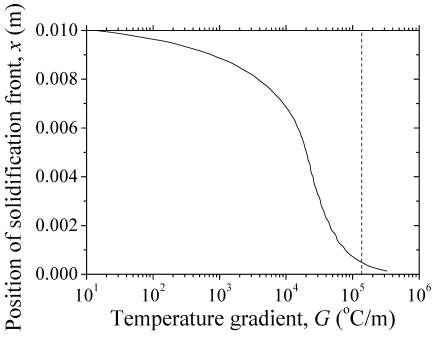

Fig. 6. Relation between moving distance of solidification front and temperature gradient. The vertical dashed line denotes the temperature gradient where the calculated *G–V* curve intersects the result of Hunt's model as shown in Fig. 5.

drite solidification developing from mold wall, which is our main concern in this study.

Figure 4 represents the time evolutions of columnar δ-dendrite tip velocity, V, and the temperature gradient at the δ/L solidification front, G. It can be seen that these quantities largely vary with the time. Although not clearly seen in this figure, the velocity sharply increases from the null value to a maximum value of approximately 0.02 m/s in the very early period. This sharp rising behavior of the velocity is ascribable to a large heat removal near the mold wall at the beginning of the casting. Then, the velocity decreases with the time down to a minimum value of approximately 1×10^{-3} m/s at $t\approx3.3$ s, followed by the gradual increment indicating an accelerating solidification process. The temperature gradient, on the other hand, remains at a very large values more than 1×10^4°C/m until $t\approx4$ s, and then it decreases quickly down to the null value in next 1.5 s. This rapid decrease in the temperature gradient results in the extension of undercooling region ahead of the columnar dendrite, which leads to the accelerating solidification process in the late period.

The relation between G and V at each time step during the casting process is indicated by the solid line in **Fig. 5**. The vertical and horizontal axes are the dendrite tip velocity, V, and the temperature gradient, G, respectively. At the very beginning of the solidification process, the velocity sharply increases under a very high temperature gradient, as shown at the right hand edge of the solid line. After such a sharp rising, two types of stages can be distinguished in this *G–V* relation. At the first stage, the velocity decreases as the temperature gradient decreases. Then, at the second stage, the velocity slightly increases with the decrease in temperature gradient which corresponds to the accelerating solidification process as described in Fig. 4. The result of the Hunt's model is shown by the dashed line in Fig. 5. This line indicates the condition of the CET of δ solidification induced by the primary Ti(C, N) particle. The undercooling for the nucleation of δ-Fe on the Ti(C, N) particle was taken to be $\Delta T_N=1.8$°C[4] and the number of the Ti(C, N) particle was given as $N_0=8\times10^{12}\,\mathrm{m}^{-3}$ which was determined from the number of the faceted particles observed in the present as-cast sample with addition of 0.15 wt% Ti. As shown in Fig. 7 of Ref. 3), there were a number of Ti(C, N) particles observed in the sample with 0.15 wt% Ti. We counted the number of the particles in the observation area to obtain the average distance between the particles, from which the number of Ti(C, N) particles in unit volume was calculated to be $N_0=8\times10^{12}\,\mathrm{m}^{-3}$. The validity of this value of N_0 is discussed later. This dashed line divides the *G–V* field into two regions; one is the lower- and right-side region for the development of the columnar dendrite structure and the other is the upper- and left-side region for the formation of fully equiaxed structure. The *G–V* curve is within the region of the columnar dendrite structure when $G>1.2\times10^5$°C/m, which corresponds to a very short period in the beginning of the solidification in Fig. 4. Then, intersecting the Hunt's criterion, the *G–V* curve goes into the region for the formation of fully equiaxed structure. In other words, after the G and V decreases to the values at the intersection point, the CET of δ solidification occurs when the Ti(C, N) particles exist in the melt.

Figure 6 demonstrates the relation between the moving distance of the solidification front and the temperature gradient. The vertical dashed line denotes the temperature gradient at which the *G–V* curve intersects with the Hunt's criterion as shown in Fig. 5. When the solidification starts at the mold wall the temperature gradient is quite high, which leads to the columnar dendrite development near the side surface of the ingot. However, the temperature gradient decreases as the solidification front migrates into the inward of the ingot and cross the vertical dashed line of the Hunt's criterion. It is quite important to note that the Hunt's criterion of the CET is satisfied just after the columnar dendrite tip migrates quite a short distance, $x=400\,\mu$m, from the

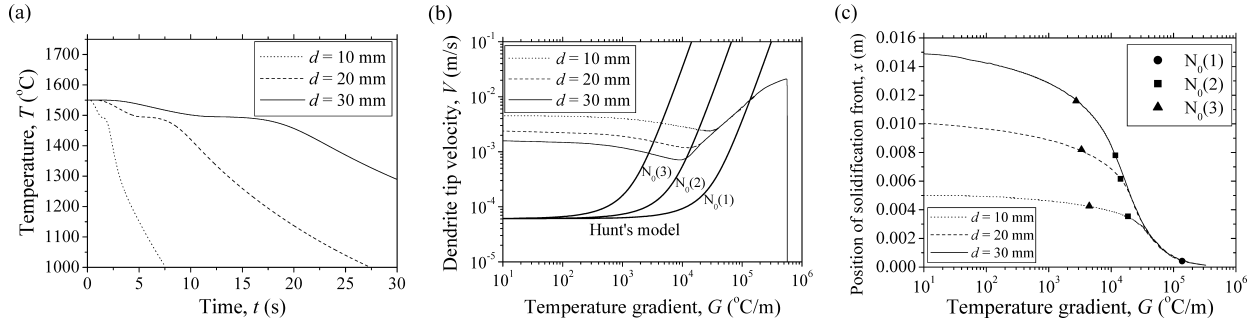

Fig. 7. Calculated results with different thickness of ingot. (a) Cooling curves at the center of sample. (b) Relations between dendrite tip velocity and temperature gradient. The bold lines represent the results of Hunt's model with $N_0(1)=8\times10^{12}$, $N_0(2)=8\times10^{10}$ and $N_0(3)=8\times10^{8}\,m^{-3}$. (c) Relations between moving position of solidification front and temperature gradient. The symbols indicate the temperature gradients at which the calculated results intersect the results of the Hunt's model.

side surface of the ingot. Hence, when the Ti(C, N) crystallizes in the melt prior to the δ solidification, the equiaxed δ dendrite forms even in the vicinity of the side surface, which is fairly consistent with the experimental evidence shown in Fig. 2. The position at which the G–V curve intersects the Hunt's criterion curve is called as the CET position in following discussion.

The present calculation indicated that the primary Ti(C, N) induces the CET of δ dendrite near the mold wall during the present casting condition. It should be pointed out that the number of the Ti(C, N) particles in the above discussion is the one determined from the microstructural observation of the as-cast ingot. It is, however, not assured that all the particles observed in the as-cast ingot acted as the heterogeneous nucleation site for the δ-dendrite and, on the other hand, there may exist finer Ti(C, N) particles which are not detectable in the resolution of our microstructural investigation. Thus, there should be an uncertainty in the above discussion regarding the effective number of Ti(C, N) particles acting as the nucleation site for the equiaxed δ-dendrite. The capability of Ti(C, N) for the CET should largely depend on the number of the Ti(C, N) particles. Such a dependency is addressed in the following. In addition, the capability of the Ti(C, N) particle for the CET is dependent on the cooling condition. In the conventional continuous casting process of the steel, the slab thickness is one of parameters affecting the cooling rate of the cast. In the following, therefore, we discuss the dependency of the CET position on the number of the Ti(C, N) particles and the cooling conditions with different thickness of ingot to clarify the capability of the Ti(C, N) for the CET.

Shown in **Fig. 7**(a) are the calculated cooling curves at the center of the ingot with different thickness of the ingot, d. One can see that the cooling rate decreases with increasing thickness of the ingot. The G–V curves during these solidification processes are given in Fig. 7(b). It is seen that the first stage exhibiting large temperature gradients of $G>5\times10^{4}$ °C/m does not considerably change depending on the ingot thickness, while the velocity V at the second stage exhibiting smaller temperature gradients decreases with the increase in ingot thickness. In Fig. 7(b), moreover, the Hunt's criterion calculated with different values of N_0, $N_0(1)=8\times10^{12}$, $N_0(2)=8\times10^{10}$ and $N_0(3)=8\times10^{8}\,m^{-3}$ are presented. As N_0 decreases, the Hunt's criterion shifts to the leftside. When $N_0=N_0(1)$, the intersection point with the Hunt's model is identical in all the cases of the different thicknesses, since there is no virtual difference in the first stage. When $N_0=N_0(2)$ or $N_0(3)$, however, the velocity and the temperature gradient at the intersection point decrease with the increase in thickness of the ingot. Figure 7(c) represents the relation between the moving position of the solidification front, x, and the temperature gradient, G. The x–G relation does not obviously change with the thickness of the ingot in the early period of the solidification, while the clear differences in x–G relation appear in the late period. The intersection points with each value of N_0 are denoted by three types of symbols as specified in the legend, which represent the CET positions. One can readily grasp that the CET position depends on the number of Ti(C, N) particles and the thickness of ingot.

Since the CET position, x_{CET}, corresponds to the distance from the mold wall to the end of the columnar dendrite region formed along the thickness direction, the fraction of the equiaxed dendrite region in the thickness direction of the ingot, f_e, can be expressed to be $f_e=1-x_{CET}/(d/2)$. **Figure 8**(a) represents the dependence of f_e on the thickness of ingot. One can see that f_e slightly increases with the increase in thickness at each value of N_0. When N_0 is small, *viz.*, $N_0=N_0(3)$, the formation of equiaxed dendrite is limited in the central region of ingot with the small fraction, $f_e\approx0.1$–0.2. However, the large number of N_0, $N_0=N_0(1)$, leads to the formation of equiaxed dendrite structure over almost the whole ingot. Figure 8(b) shows the dependence of f_e on the number of particles, N_0, at each value of thickness. It is noted that starting from nearly null value at small value of N_0, f_e drastically increases with N_0 in the range between $N_0=10^{11}$ and $10^{13}\,m^{-3}$ and, then, it asymptotically approaches 1.0 when $N_0>10^{13}\,m^{-3}$ in each case of the different thickness. Therefore, a sufficient number of Ti(C, N) particles results in the formation of equiaxed structure over the whole ingot regardless of the thickness of the cast ingot. This result indicates the high ability of Ti(C, N) giving rise to the CET.

5. Summary

In this study, the dendrite growth simulations were performed to analyze the CET of δ-dendrite solidification induced by the primary Ti(C, N) crystal. The following important results are demonstrated.

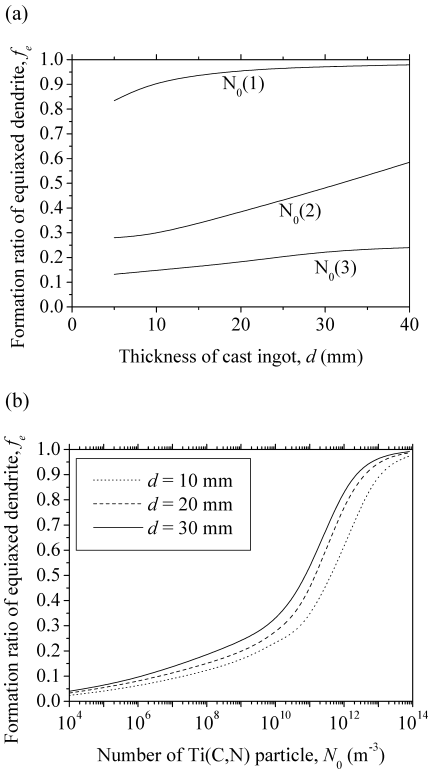

Fig. 8. (a) Dependence of the fraction of equiaxed dendrite region on the thickness of cast ingot. (b) Dependence of the fraction of equiaxed dendrite on the number of Ti(C, N) particles.

(1) The relation between the calculated *G–V* relation and the Hunt's criterion suggests that the Ti(C, N) particle gives rise to the CET of δ solidification even in the vicinity of the side surface of the ingot under the present casting condition. This is fairly consistent with the experimental result.

(2) A sufficient number of Ti(C, N) particles of $N_0 > 10^{13}\,m^{-3}$ lead to the formation of equiaxed structure even at the side surface of the ingot regardless of the size of the cast ingot.

Acknowledgement

This work is partially supported by the Next Generation Super Computing Project, Nanoscience Program, MEXT, Japan.

REFERENCES

1) Y. Maehara, K. Yasumoto, Y. Sugitani and K. Gunji: *Tetsu-to-Hagané*, **71** (1985), 1534.
2) L. Schmidt and A. Josefsson: *Scand. J. Metall.*, **3** (1974), 193.
3) M. Ohno and K. Matsuura: *ISIJ Int.*, **48** (2008), 1373.
4) B.L. Bramfitt: *Metall. Trans.*, **1** (1970), 1987.
5) K. Nakajima, H. Hasegawa, S. Khumkoa and S. Mizoguchi: *Metall. Mater. Trans. B*, **34B** (2003), 539.
6) K. Isobe, M. Kusano and K. Hirabayashi: *CAMP-ISIJ*, **10** (1997), 973.
7) T. Koseki and H. Inoue: *J. Jpn. Inst. Met.*, **65** (2001), 644.
8) J. D. Hunt: *Mater. Sci. Eng.*, **65** (1984), 75.
9) M. Gaumann, R. Trivedi and W. Kurz: *Mater. Sci. Eng. A*, **226** (1997), 763.
10) C. Y. Wang and C. Beckermann: *Metall. Mater. Trans. A*, **27A** (1996), 4217.
11) M. A. Martorano, C. Beckermann and C. A. Gandin: *Metall. Mater. Trans. A*, **34A** (2003), 1657.
12) A. Badillo and C. Beckermann: *Acta Mater.*, **54** (2006), 2015.
13) M. Vandyoussefi and A. L. Greer: *Acta Mater.*, **50** (2002), 1693.
14) H. B. Dong and P. D. Lee: *Acta Mater.*, **53** (2005), 659.
15) M. Wu and A. Ludwig: *Metall. Mater. Trans A*, **37A** (2006), 1613.
16) W. Kurz, C. Bezençon and M. Gäumann: *Sci. Technol. Adv. Mater.*, **2** (2001), 185.
17) M. Rappaz and Ch.-A. Gandin: *Acta Metall. Mater.*, **41** (1993), 345.
18) Ch.-A. Gandin and M. Rappaz: *Acta Metall. Mater.*, **42** (1994), 2233.
19) W. Kurz, B. Giovanola and R. Trivedi: *Acta Metall.*, **34** (1986), 823.
20) W. W. Mullins and R. F. Sekerka: *J. Appl. Phys.*, **35** (1964), 444.
21) P. Gustafson: *Scand. J. Metall.*, **14** (1985), 259.
22) E. Scheil: *Z. Metallkd.*, **34** (1942), 70.
23) A. Suzuki, T. Suzuki, Y. Nagaoka and Y. Iwata: *J. Jpn. Inst. Met.*, **32** (1968), 1301.
24) W. Kurz and D. J. Fisher: Fundamentals of Solidification, Trans. Tech. Publication, Switzerland, (1989).
25) The Japan Institute of Metals: Kinzoku Databook, 4th edition, Maruzen, Japan, (2004).